PERGAMON

International Journal of Solids and Structures 37 (2000) 835–856

INTERNATIONAL JOURNAL OF SOLIDS and STRUCTURES

www.elsevier.com/locate/ijsolstr

# Energy release rate along any crack front in the thickness direction of shell elements

X.Z. Suo[a,*], M.P. Valeta[b], B. Drubay[b], B. Martelet[c], H. Deschanels[d]

[a]*EUROSIM SARL, Centre d'Affaires, 2 Rue de la Renaissance, 92160 Antony, Cedex France*
[b]*CEA/DMT/SEMT/LAMS, 91191 Gif Sur Yvette, France*
[c]*EDF/SEPTEN, 12–14 Avenue Dutrièvoz, 69628 Villeurbanne, France*
[d]*NOVATOME–FRAMATOME, 10 Rue Juliette Récamier, 69006 Lyon, France*

Received 31 July 1997; in revised form 30 March 1999

**Abstract**

This paper deals with a numerical method for calculating the profile of the energy release rate $G$ (or $J$-integral) along any crack front in the thickness direction of shell elements. For this purpose, the virtual crack extension technique is firstly used for its average evaluation throughout the entire shell thickness. Secondly, local values for points on the crack front are derived by assuming that the $G$ parameter at any level in the shell's thickness direction is linearly proportional to the strain energy density of points at the same level in the region where HRR singular fields are dominant. Example computations show that the $G$ parameter profile by the present method is in good agreement with that by alternative methods throughout a large range of elastic–plastic deformation. 

*Keywords:* Energy release rate; J-integral; Virtual crack extension; HRR singular fields; 3D crack front; Multi-layer shell elements

## 1. Introduction

When the material around a crack front undergoes a substantial amount of plastic flow, it has become common to characterize the static crack initiation and subsequent crack growth under monotonically increasing deformation condition by using the energy release rate, $G$, (or the $J$-integral). It is, therefore, important to have access to techniques for calculating this fracture parameter under elastic–plastic conditions for both 2D and 3D crack configurations. These techniques should be based on a solid continuum mechanics formulation, be sufficiently general to cover a variety of structure configurations, and be relatively easy to use. Two different methods presently widely mentioned in the literature satisfy these

* Corresponding author. Fax: +33-1-5559-9636.

0020-7683/00/$ - see front matter 
PII: S0020-7683(99)00105-5

conditions. The first of these is the *J*-integral method, which is based on a path independent surface integral (line integral for 2D crack problems); the second is the virtual crack extension (or VCE) technique introduced independently by Parks (1974) and Hellen (1975), which models the crack extension by a small shift of node points in the finite element model.

For 3D cases in the presence of body forces or thermal loadings, the *J*-integral technique consists of an integration over a surface around a particular point on the crack front, and also a volume integration performed over the volume enclosed by the surface. In the finite element framework, this integration surface is in general difficult to define and the surface integration is itself delicate to perform. In contrast with the *J*-integral technique, the VCE method allows the energy release rate to be computed, always by a volume integration, through a small computation effort. If a numerical analysis is carried out by the finite element method, the volume integration formulation of the VCE method is preferable to the surface integration formulation because the former is a natural extension of the volume integrals already carried out in the finite element programs. For this reason, the VCE method has received a wider attention in our research work (Suo and Combescure, 1992a) and, in the literature, a great deal of effort has also been devoted both to its theoretical developments and numerical applications (Haber and Koh, 1985; Parks, 1977; Ishikawa, 1980; Nikishkov and Atluri, 1987; Pryor et al., 1970; Sha and Yang, 1985; Hellen, 1989). From the fact that the earlier formulations of the VCE method were only based on a finite element approach (the resulting formula is hence written in finite element matrix form), Destuynder and Djaoua (1981) and De Lorenzi (1982) have derived an explicit 3D analytical expression for the energy release rate by the application of the VCE principle to a continuum mechanics model.

For crack geometries modeled by 3D solid elements, the virtual crack extensions are usually conducted by a small node movement in the direction normal to the crack front. The profile of the energy release rate along this line will be yielded by repeating such a movement node by node (Suo and Combescure, 1992b). A movement of all these nodes together leads to a value which emerges as an integration of the above *G* profile over the crack front, and may be regarded as an average evaluation of the *G* parameter. When using shell elements for thin walled structures where the crack front is modeled by a single node on structure's middle surface, the value deduced from the crack-tip movement is an average one throughout the entire shell thickness. The traditional VCE method cannot provide the local value of the *G* parameter at any particular level in the shell thickness, hence the profile of the energy release rate, because of the absence of intermediate nodal points in this direction. In the case where the membrane strain in the shell elements is preponderant, the energy release rate is nearly constant throughout the entire crack front. Therefore, the knowledge of its average value would be representative enough, as has been done in our earlier work (Suo and Combescure, 1992b). However, in the case where shell elements are subjected to a substantial amount of bending strain, the *G* parameter varies in the shell's thickness, so that an evaluations of the energy release rate profile all along the crack front should be of great importance, even imperative, to determine where the stress singularities are strongest.

The aim of the present paper is to present a numerical method for calculating the profile of the energy release rate (or the *J*-integral) along any crack front in the thickness direction of shell elements. For this purpose, it is assumed that the energy release rate at any level in the crack front is linearly proportional to the strain energy density of points at the same level in the region where HRR singular fields (Hutchinson, 1968; Rice and Rosengren, 1968) are dominant. Firstly, the VCE method is used to provide an average estimation of the energy release rate throughout the entire shell thickness. Secondly, local values in the crack front are derived by means of an interpolation of the resulting average value with a function representing the evolution of the strain energy density in the thickness direction of shell elements. Example computations are presented in the final section of the paper and compared against reference solutions for an elastic and an elastic–plastic crack problems as well.

## 2. Average energy release rate

An explicit 3D analytical expression for the energy release rate, $G$, was derived in the work by Destuynder and Djaoua (1981) and independently in that by De Lorenzi (1982) for linear elastic materials and for materials following the deformation theory of plasticity, respectively. In the absence of surface tractions on the crack faces and thermal loadings, it was found to be:

$$\Delta AG = \int_{\Omega} \mathrm{Tr}(\sigma \nabla U \nabla \Theta) \mathrm{d}\Omega - \frac{1}{2}\int_{\Omega} w \,\mathrm{div}\, \Theta \,\mathrm{d}\Omega. \tag{1}$$

In this expression, $\Delta A$ is the increase in cracked area generated by a small node movement, $\Omega$ is the volume of the cracked body, $\sigma_{ij}$ is the stress tensor, $U_i$ is the displacement vector and $w$ is the strain energy density. 'Tr' denotes trace operation for tensors and $\Theta$ is a mapping function which maps the body containing the crack into a body with a slightly increased crack length. In the calculations of the energy release rate by Eq. (1), a Cartesian coordinate system $x_i$ and the index notation with the summation convention for repeated indices should be used.

If a shell analysis is performed by the finite element method, the above formula for the energy release rate has to be put into the finite element framework. Usually, the formulations of shell elements are carried out by using the generalized Kirchhoff hypothesis which states that:

> *points in a shell originally on the normal to the undeformed middle surface remain on a straight line, but which is not necessarily yet normal to the deformed middle surface.*

Under the hypothesis of small displacement and small strain, this allows us to write the displacement components of a point in the local Cartesian coordinate system $(x, y, z)$ of the shell elements as follows:

$$U = U_x(x, y, 0) + z\beta_x(x, y),$$

$$V = U_y(x, y, 0) + z\beta_y(x, y),$$

$$W = U_z(x, y)$$

where the $x$–$y$ plane represents the shell's middle surface, $z$ the axis in the thickness direction of the shell elements, orthogonal to the middle surface $x$–$y$. $U_x$ and $U_y$ are membrane displacement components in the $x$-axis and $y$-axis directions, $\beta_x$, and $\beta_y$ are two rotations of the normal to the undeformed middle surface in the $x$–$z$ and $y$–$z$ planes, $U_z$ is the transversal displacement in the $z$-axis direction. In the analyses of shell elements including the transverse shear energy, the strain is divided into three terms: membrane strain, $\varepsilon^{\mathrm{m}}$, bending strain, $\varepsilon^{\mathrm{b}}$ and transversal shear strain, $\varepsilon^{\mathrm{s}}$, which are written in vector form as follows:

$$\varepsilon^{\mathrm{m}} = \left[\frac{\partial U_x}{\partial x}\frac{\partial U_y}{\partial y}\frac{\partial U_x}{\partial y} + \frac{\partial U_y}{\partial x}\right]^{\mathrm{T}},$$

$$\varepsilon^{\mathrm{b}} = z\mathbf{k} \text{ with } \mathbf{k} = \left[\frac{\partial \beta_x}{\partial x}\frac{\partial \beta_y}{\partial y}\frac{\partial \beta_x}{\partial y} + \frac{\partial \beta_y}{\partial x}\right]^{\mathrm{T}}$$

$$\varepsilon^{s} = \left[\beta_x + \frac{\partial U_z}{\partial x}\beta_y + \frac{\partial U_z}{\partial y}\right]^{T},$$

with 'T' denoting transpose. In elasticity, these strain fields are connected to the membrane stress, $\sigma^{m}$, bending stress, $\sigma^{b}$ and transversal shear stress, $\sigma^{s}$, by:

$$\sigma^{m} = \mathbf{D}\varepsilon^{m},$$

$$\sigma^{s} = \mathbf{D}^{s}\varepsilon^{s},$$

$$\sigma^{b} = \mathbf{zDk}, \tag{2}$$

where $\mathbf{D}$ is the elastic constitutive matrix and $\mathbf{D}^{s}$ is the elastic shear matrix. In shell element calculations, the total membrane force, $\mathbf{N}$, shear force, $\mathbf{T}$, and bending moment, $\mathbf{M}$, obtained through an integration of the above stresses over the shell thickness are often more representative:

$$\mathbf{N} = e\sigma^{m} = e\mathbf{D}\varepsilon^{m},$$

$$\mathbf{T} = e\sigma^{s} = e\mathbf{D}^{s}\varepsilon^{s},$$

$$\mathbf{M} = \frac{e^3}{12z}\sigma^{b} = \frac{e^3}{12}\mathbf{Dk}, \tag{3}$$

where $e$ is the shell's thickness.

With the definition of the mapping function (Destuynder and Djaoua, 1981; De Lorenzi, 1982; Suo and Combescure, 1992b) and, particularly for an average evaluation of the energy release rate, it is reasonable to assume that the displacement vector $\Theta$ does not vary in the $z$-axis thickness direction of shell elements, namely in the local Cartesian coordinate system $(x, y, z)$ we have:

$$\Theta_x = \Theta_x(x, y),$$

$$\Theta_y = \Theta_y(x, y),$$

$$\Theta_x = 0.$$

This assumption allows the two integrals in the right hand side of Eq. (1) to be explicited in term of the displacement and effort components in shell elements:

$$\Delta AG_1 = \frac{1}{2}\int_S \mathrm{Tr}(\sigma\nabla\mathbf{U})\mathrm{div}\,\Theta\,\mathrm{d}\Omega = \frac{1}{2}\int_S [\mathbf{N}^{T}\varepsilon^{m} + \mathbf{T}^{T}\varepsilon^{s} + \mathbf{M}^{T}\mathbf{k}]\mathrm{div}\,\Theta\,\mathrm{d}S, \tag{4}$$

$$\Delta AG_2 = \int_S \mathrm{Tr}(\sigma\nabla\Theta\nabla\mathbf{U})\mathrm{d}\Omega = \int_S [\mathbf{N}^{T}\varepsilon^{m}(\mathbf{U}, \Theta) + \mathbf{T}^{T}\varepsilon^{s}(\mathbf{U}, \Theta) + \mathbf{M}^{T}\mathbf{k}(\mathbf{U}, \Theta)]\mathrm{d}S, \tag{5}$$

where integrations should be carried out in the local coordinate system of each element. In the above expressions, $S$ is the surface of the middle plane, $\varepsilon^{m}(\mathbf{U}, \Theta)$, $\varepsilon^{c}(\mathbf{U}, \Theta)$ and $\mathbf{k}(\mathbf{U}, \Theta)$ are the membrane, transversal shear and bending strains associated with the mapping $\Theta$. They are written as:

$$\varepsilon^{m}(\mathbf{U},\,\Theta)=\begin{bmatrix} U_{x,x}\Theta_{x,x}+U_{x,y}\Theta_{y,x} \\ U_{y,x}\Theta_{x,y}+U_{y,y}\Theta_{y,y} \\ U_{x,x}\Theta_{x,y}+U_{x,y}\Theta_{y,y}+U_{y,x}\Theta_{x,x}+U_{y,y}\Theta_{y,x} \end{bmatrix},$$

$$\varepsilon^{s}(\mathbf{U},\,\Theta)=\begin{bmatrix} U_{z,x}\Theta_{x,x}+U_{z,y}\Theta_{y,x} \\ U_{z,x}\Theta_{x,y}+U_{z,y}\Theta_{y,y} \end{bmatrix},$$

$$\mathbf{k}(\mathbf{U},\,\Theta)=\begin{bmatrix} \beta_{x,x}\Theta_{x,x}+\beta_{x,y}\Theta_{y,x} \\ \beta_{y,x}\Theta_{x,y}+\beta_{y,y}\Theta_{y,y} \\ \beta_{x,x}\Theta_{x,y}+\beta_{x,y}\Theta_{y,y}+\beta_{y,x}\Theta_{x,x}+\beta_{y,y}\Theta_{y,x} \end{bmatrix}.$$

By using the divergence theorem, it may be shown that the average energy release rate computed by the sum of Eqs. (4) and (5) is identical to the 2D plane stress line independent $J$-integral. This means that the $G$ parameter is itself independent of the displacement vector $\Theta$ when the latter is directed to the crack-axis direction (Suo and Combescure, 1992b).

## 3. Energy release rate along the crack front

For calculating the energy release rate at any particular level in the thickness direction of shell elements, it is convenient to use the results that we can deduce immediately from the HRR singular fields of stress and strain in the neighborhood of the crack tip. For materials following the deformation theory of plasticity, they were found to be (Hutchinson, 1968; Rice and Rosengren, 1968):

$$\frac{\sigma_{ij}}{\sigma_y}(r,\,\theta)=\left(\frac{JE}{I\alpha\sigma_y^2 a}\right)^{1/(n+1)}\frac{\tilde{\sigma}_{ij}(\theta)}{(r/a)^{1/(n+1)}},$$

$$\frac{\varepsilon_{ij}}{\varepsilon_y}(r,\,\theta)=\alpha\left(\frac{JE}{I\alpha\sigma_y^2 a}\right)^{n/(n+1)}\frac{\tilde{\varepsilon}_{ij}(\theta)}{(r/a)^{n/(n+1)}},$$

where $n$ and $\alpha$ are the work hardening exponent and the yield offset, introduced in the Ramberg–Osgood $\sigma$–$\varepsilon$ relationship, $I$ is a dimensionless parameter depending only on $n$, $a$ is the crack length, $E$ is the Young's modulus, $(r,\,\theta)$ are cylindrical coordinates of points in a crack-tip coordinate system, and are two functions of angle $\theta$. The strain energy density is, therefore, simply:

$$w=\sigma_{ij}\varepsilon_{ij}=\frac{\tilde{\sigma}_{ij}(\theta)\tilde{\varepsilon}_{ij}(\theta)}{Ir}J=\lambda J,$$

with

$$\lambda=\frac{\tilde{\sigma}_{ij}(\theta)\tilde{\varepsilon}_{ij}(\theta)}{Ir}. \tag{6}$$

For shell elements, it seems reasonable to assume that the factor $\lambda$ in Eq. (6) is independent of the coordinate $z$ in the thickness direction. This hypothesis leads to the conclusion that the energy release rate (or the $J$-integral) at any level in the crack front is linearly proportional to the strain energy density $w$ of points at the same level in the HRR-field controlled region. Physically, this means that the

behaviour of cracks in a thin structure is govened directly by the strain energy density. The possible growth of a crack front will happen at the point where the strain energy density is strongest.

In elasticity, the energy release rate should be a quadratic function over the thickness of the shell element since both stress and strain vary linearly in such a direction. This implies that, in elasticity, we can write:

$$G(z) = \left[ A\left(\frac{z}{e}\right)^2 + B\left(\frac{z}{e}\right) + C \right] G, \tag{7}$$

where $G$ is the average energy release rate over the whole crack front and calculated by the sum of Eqs. (4) and (5), $A$, $B$ and $C$ are three dimensionalless constants to be determined below. Let the strain energy density on the shell's middle plane, top and bottom surfaces be represented, respectively, by $w_0$, $w_1$ and $w_2$. Note that at any level, $z$, in the shell's thickness, the strain energy dentity $w(z)$ may be computed by a simple product of stress and strain, giving:

$$w(z) = \left( \frac{\mathbf{N}}{e} + \frac{12\mathbf{M}z}{e^3} \right)(\varepsilon^{\mathrm{m}} + z\mathbf{k}) + \frac{\mathbf{T}}{e}\varepsilon^{\mathrm{s}}. \tag{8}$$

The proportional assumption introduced previously permits to write:

$$\frac{1}{4}A + \frac{1}{2}B + C = C\frac{w_1}{w_0}, \tag{9}$$

$$\frac{1}{4}A - \frac{1}{2}B + C = C\frac{w_2}{w_0}. \tag{10}$$

In addition, since the energy release rate is a linear function of the mapping vector $\Theta$ which is, itself, assumed to be constant in the thickness direction, an integration of the $G$ profile Eq. (7) over the element thickness must lead to the average energy release rate, $G$, throughout the whole crack front, namely:

$$\int_{-e/2}^{+e/2} G(z)\mathrm{d}z = eG. \tag{11}$$

Substituting Eq. (7) into Eq. (11) gives another equality:

$$\frac{1}{12}A + C = 1. \tag{12}$$

By resolving Eqs. (9), (10) and (12), the constants $A$, $B$ and $C$ are found to be:

$$A = 12\frac{\dfrac{w_1}{w_0} + \dfrac{w_2}{w_0} - 2}{\dfrac{w_1}{w_0} + \dfrac{w_2}{w_0} + 4}, \tag{13}$$

$$B = 6\frac{\dfrac{w_1}{w_0} - \dfrac{w_2}{w_0}}{\dfrac{w_1}{w_0} + \dfrac{w_2}{w_0} + 4} \tag{14}$$

$$C = \frac{6}{\frac{w_0}{w_1} + \frac{w_0}{w_2} + 4}. \tag{15}$$

By substituting the constants $A$, $B$ and $C$ into Eq. (7), it follows the energy release rate profile along the crack front in the thickness direction of shell elements:

$$G(z) = \frac{6G}{\frac{w_1}{w_0} + \frac{w_2}{w_0} + 4}\left[2\left(\frac{w_1}{w_0} + \frac{w_2}{w_0} - 2\right)\frac{z^2}{e^2} + \left(\frac{w_1}{w_0} - \frac{w_2}{w_0}\right)\frac{z}{e} + 1\right]. \tag{16}$$

Again, it should be emphasized that the calculations of the strain energy densities by Eq. (8) for $w_0$ with $z = 0$, for $w_1$ with $z = e/2$ and for $w_2$ with $z = -e/2$ have to be performed for points in the HRR-field controlled region near the crack tip.

Almost all thin plate/shell models developed in the literature accept the normal or generalized Kirchhoff hypothesis, i.e. a linear strain variation in the thickness direction of shell elements both for linear elastic materials and elastic–plastic materials as well. However, in the latter case, stress varies non linearly in such a direction, following the material's stress–strain curve. For instance, the energy release rate of materials of the Ramberg–Osgood type having $n$ as its work hardening exponent should vary non linearly according to a power function of $(n + 1)$ order. It is clear that if a polynomial function is always introduced in this case for an exact evaluation of the energy release rate, we have to find $(n + 2)$ constants rather than 3 in the preceding elasticity situation. To simplify calculations and, particularly, for the assessment of a technique covering a wider class of non linear material models, it seems more advantageous to approximate the energy release rate profile by means of a strain energy density $w(z)$ at some finite levels in shell's thickness. More clearly, since Eq. (11) is pertinent in linear elasticity as well as in elastic–plasticity, substituting Eq. (6) into Eq. (11) yields:

$$G(z) = \frac{eGw(z)}{\int_{-e/2}^{+e/2} w(z)\mathrm{d}z}. \tag{17}$$

In elastic–plasticity, two different approachs are available to determine the strain energy density at any particular level in the thickness of shell elements. The first of these is the numerical integration method in the shell's thickness (Batoz and Dhatt, 1990) which allows the strain and stress at any specified levels in the thickness to be computed through a small calculation effort. The second is the multi-layer element model used in this paper for the example calculations, which requires just a single element in the HRR-field controlled region being modeled with $(2N + 1)$ layers having equal and sufficiently slim thickness (see Fig. 1).

A brief presentation of such an element model is given below, proving that the use of Eq. (17) may lead to results very close to those by Eq. (16) in elasticity. Also, such a demonstration provides a numerical process of the use of Eq. (17) in elasto–plastic cases. For this purpose, let each layer in Fig. 1 be characterized by a very small thickness $e_i$ (identical for all layers) and an eccentricity $\lambda_i$. The displacement in a particular layer $i$ is divided into two distinct parts:

$$U_i^{\mathrm{m}} = U_x(x, y) + \lambda_i \beta_x(x, y),$$

$$V_i^{\mathrm{m}} = U_y(x, y, 0) + \lambda_i \beta_y(x, y)$$

$$W_i^{\mathrm{m}} = 0,$$

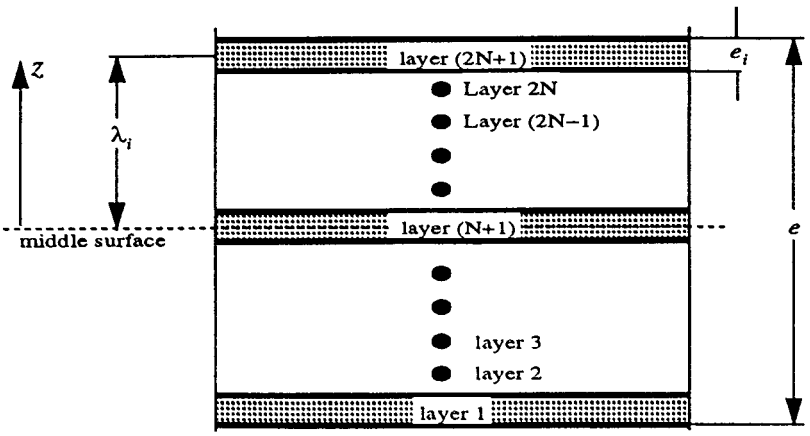


Fig. 1. Multi-layer model for a single element in the HRR-field controlled region.

for the membrane displacement components in the shell's middle surface and

$$U_i^f = (z - \lambda_i)\beta_x(x, y),$$

$$V_i^f = (z - \lambda_i)\beta_y(x, y),$$

$$W_i^f = U_z(x, y),$$

for the displacement components due to the normal vector rotations with respect to the undeformed middle surface. Also, the strain in the layer $i$ is divided into membrane strain, $\varepsilon_i^{\mathrm{m}}$, bending strain, $\varepsilon_i^{\mathrm{b}}$ and transversal shear strain, $\varepsilon_i^{\mathrm{s}}$:

$$\varepsilon_i^{\mathrm{m}} = \varepsilon^{\mathrm{m}} + \lambda_i \mathbf{k},$$

$$\varepsilon_i^{\mathrm{b}} = (z - \lambda_i)\mathbf{k},$$

$$\varepsilon_i^{\mathrm{s}} = \varepsilon^{\mathrm{s}}. \tag{18}$$

In elasticity, the corresponding membrane stress, $\sigma_i^{\mathrm{m}}$, bending stress, $\sigma_i^{\mathrm{b}}$ and the shear stress, $\sigma_i^{\mathrm{s}}$, are respectively:

$$\sigma_i^{\mathrm{m}} = \mathbf{D}\varepsilon_i^{\mathrm{m}},$$

$$\sigma_i^{\mathrm{b}} = \mathbf{D}\varepsilon_i^{\mathrm{b}},$$

$$\sigma_i^{\mathrm{s}} = \mathbf{D}^{\mathrm{s}}\varepsilon_i^{\mathrm{s}}. \tag{19}$$

Similarly, the total membrane forces, $\mathbf{N}_i$, transversal shear forces, $\mathbf{T}_i$, and bending moments, $\mathbf{M}_i$, with respect to the middle surface of each individual layer $i$ may be derived by means of an integration of the

above stresses over the thickness $e_i$:

$$\mathbf{N}_i = \int_{\lambda_i - e_i/2}^{\lambda_i + e_i/2} \left(\sigma_i^{\mathrm{m}} + \sigma_i^{\mathrm{b}}\right) \mathrm{d}z = e_i \mathbf{D} \varepsilon^{\mathrm{m}} + e_i \mathbf{D} \lambda_i \mathbf{k}, \tag{20}$$

$$\mathbf{M}_i = \int_{\lambda_i - e_i/2}^{\lambda_i + e_i/2} (\mathbf{z} - \lambda_i)\left(\sigma_i^{\mathrm{m}} + \sigma_i^{\mathrm{b}}\right) \mathrm{d}z = \frac{e_i^3}{12} \mathbf{D} \mathbf{k}, \tag{21}$$

$$\mathbf{T}_i = \int_{\lambda_i - e_i/2}^{\lambda_i + e_i/2} \sigma_i^{\mathrm{s}} \, \mathrm{d}z = e_i \mathbf{D}^{\mathrm{s}} \varepsilon^{\mathrm{s}}. \tag{22}$$

The total strain energy, $W(\lambda_i)$, at layer $i$ is computed by:

$$W(\lambda_i) = \int_{\lambda_i - e_i/2}^{\lambda_i + e_i/2} \sigma_i \varepsilon_i \, \mathrm{d}z.$$

By substituting Eqs. (18) and (19) into the right hand side of the above equation, we easily obtain

$$W(\lambda_i) = \mathbf{N}_i \varepsilon_i^{\mathrm{m}} + \mathbf{T}_i \varepsilon^{\mathrm{s}} + \mathbf{M}_i \mathbf{k}. \tag{23}$$

Alternatively, since the thickness of all layers is very small compared to the total shell thickness ($e_i/e \ll 1$), the eccentricity $\lambda_i$ may be regarded here as the $z$ coordinate of points in the thickness. It follows that in elasticity, Eq. (23) may also be written as:

$$W(\lambda_i) = e_i \left[ \left( \frac{\mathbf{N}}{e} + \frac{12\mathbf{M}z}{e^3} \right)(\varepsilon^{\mathrm{m}} + z\mathbf{k}) + \frac{\mathbf{T}}{e} \varepsilon^{\mathrm{s}} \right] + \frac{e_i^3}{e^3} \mathbf{M} \mathbf{k}. \tag{24}$$

Since $e_i/e \ll 1$, the contribution of the bending moment $\mathbf{M}$ in the last term of Eq. (24) may be ignored so that we can replace the energy density $w(z)$ in Eq. (17) by, approximately, the total strain energy $W(z)$:

$$G(z) = \frac{eGw(z)}{\int_{-e/2}^{+e/2} w(z) \mathrm{d}z} = \frac{eGW(\lambda_i)}{\int_{-e/2}^{+e/2} W(\lambda_i) \mathrm{d}z}. \tag{25}$$

Eq. (25) is true only if all layers have the same thickness $e_i$. It is worthwhile to point out that the calculations with Eq. (23) or Eq. (24) in elasticity have to be repeated for all layers in the element in order to establish $(2N + 1)$ one-to-one relationships between $W(\lambda_i)$ and the $z$ coordinate (replaced here by the layer's eccentricity $\lambda_i$). The second denominator in Eq. (25) is then replaced approximately by the area below the $W(\lambda_i)$–$z$ curve composed of $2N$ piece-wise straight lines. Numerically, this area may be computed without any particular difficulties by using, for instance, the trapeze integration method. Of course, the number of multi-layers in the element must be enough to guarantee that the resulting area is sufficiently close to that below the theoretical smooth $W(\lambda_i)$–$z$ curve. Compared to the average energy release rate by the classic VCE method (Suo and Combescure, 1992b), the proposed method should not make the computation effort much heavier since the multi-layer model is built for a single element alone.

In the finite element applications, three matrices, $[\mathbf{B}_i^{\mathrm{m}}]$, $[\mathbf{B}_i^{\mathrm{b}}]$ and $[\mathbf{B}_i^{\mathrm{s}}]$, are commonly introduced which connect, respectively, the membrane strain, $\varepsilon_i^{\mathrm{m}}$, the bending strain, $\varepsilon_i^{\mathrm{b}}$ and the transversal shear strain, $\varepsilon_i^{\mathrm{s}}$, of each individual layer to the nodal displacement $[\mathbf{U}]$:

$$\varepsilon_i^{\mathrm{m}} = \left[\mathbf{B}_i^{\mathrm{m}}\right][\mathbf{U}],$$

$$\varepsilon_i^{\mathrm{b}} = \left[\mathbf{B}_i^{\mathrm{b}}\right][\mathbf{U}],$$

$$\varepsilon_i^{\mathrm{s}} = \left[\mathbf{B}_i^{\mathrm{s}}\right][\mathbf{U}]. \tag{26}$$

The individual stiffness matrix $[\mathbf{K}_i]$ is simply:

$$[\mathbf{K}_i] = \int_A \left[ e_i \left[\mathbf{B}_i^{\mathrm{m}}\right]^{\mathrm{T}} [\mathbf{D}] \left[\mathbf{B}_i^{\mathrm{m}}\right] + \frac{e_i^3}{12} \left[\mathbf{B}_i^{\mathrm{b}}\right]^{\mathrm{T}} [\mathbf{D}] \left[\mathbf{B}_i^{\mathrm{b}}\right] + e_i \left[\mathbf{B}_i^{\mathrm{s}}\right]^{\mathrm{T}} [\mathbf{D}] \left[\mathbf{B}_i^{\mathrm{s}}\right] \right] \mathrm{d}A. \tag{27}$$

Then, the nodal displacement resolution may be accomplished by a normal run with the master stiffness matrix assembled from each individual stiffness matrix.

The numerical process described above aims at a linear elastic case. It is seen that each individual layer behaves as an independent entity so that we can treat the layers in Fig. 1 as independent elements in the direction of shell thickness. Also, experience gained in program writing show that subroutines used in elastic–plasticity for normal mono-layer shell elements remain almost totally suitable for the multi-layer element model without any major modifications. However, in non linear material cases, the quantity $W(\lambda_i)$ must be integrated over the applied loading history in order to deduce the strain energy of layer $i$ at a given time. Numerically, this is usually done with the rapeze integration method:

$$W(\lambda_i) = \int_0^t W(\lambda_i, t)\mathrm{d}t = \frac{1}{2} \sum_{j=0}^{j(t)} \int_{\lambda_i - e_i/2}^{\lambda_i + e_i/2} (\sigma_i \varepsilon_i)_{j+1} - \int_{\lambda_i - e_i/2}^{\lambda_i + e_i/2} (\sigma_i \varepsilon_i)_j.$$

The elastic–plastic applications of the multi-layer shell element model will not be discussed more profoundly because it is not the main object of the present paper. The Reader may refer to any finite element books for more information about this subject.

## 4. Numerical illustrations

To benchmark the method described in the preceding sections, the $J$-integral profile along the crack front was computed for a through-wall flawed plate problem in elasticity as well as in elastic–plasticity using the *CASTEM2000* finite element system. Mainly, the analyses were performed with COQ8 shell elements, including transverse shear effects (eight nodal points and eight integration points for each element). Computed solutions were compared either against the analytical solutions, or against those deduced from a 3D brick element model by using the classic VCE method, namely the node-by-node extensions of all nodal points on the crack front. All calculations were carried out in double precision on a Silicon Indigo-2 computer.

### *4.1. Elastic through-wall flawed plate subjected to remote tension*

Fig. 2 shows the thin plate containing a through-wall crack with total length of $2a$ (35 mm). $e$ (28 mm) is the plate thickness, $2W$ (140 mm) the total plate width, $2L$ (280 mm) the total plate length. The remaining ligament on each side of the crack is $(W-a)$. Firstly, the loading is considered to be due to a pure membrane tension, $F$, uniformly applied at the ends in such a manner that an equal stress, 10 Mpa, is obtained throughout the whole plate transversal section. The membrane tension $F$ itself is therefore:

$$F = 2We \times 10 = 3.92 \times 10^4 \text{ N}.$$

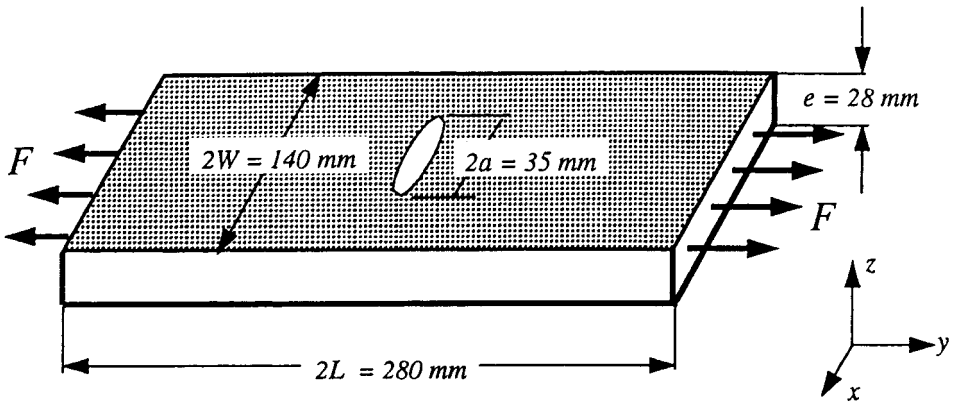


Fig. 2. Flawed plate subjected to a pure membrane tension.

In elasticity, the material is characterized by Young's modulus $E$ ($2 \times 10^5$ Mpa) and by Poisson's coefficient $\nu$ (0.3). Owing to symmetry reasons, only a quarter of the plate was analyzed. The finite element model is built with 465 eight-noded shell elements and 1430 nodal points (see Fig. 3). In calculations, symmetry boundary conditions were made on the symmetry faces and the membrane-tension-applied faces were simply locked in the thickness direction of the plate. Analytical solution for the $J$-integral has been found to be (Isida, 1955):

$$J = \frac{1}{E}\sigma^2 \pi a f^2\left(\frac{a}{W}, \frac{L}{W}\right).$$

Following Isida (1955), the factor $f$ for this problem equals 1.04, hence $J = 2.973 \times 10^{-2}$ N/mm.

Under pure membrane tension, the $G$ parameter is constant throughout the whole transversal section. This point should be verified by the method presented in the paper. On the other hand, the $G$ parameter calculations require the selection of an element row surrounding the crack tip, in which the $\Theta$ mapping vector varies gradually. The fact that the $J$ line integral is independent of integration paths implies that the $G$ parameter is itself independent of the $\Theta$ mapping vector. It is possible to define several element rows and all these selections should, theoretically, lead to the same $G$ profile along the crack front. However, in numerical analysis, there will always be some scatter in the results. In order to illustrate the independence of the computed $G$ profile with respect to the $\Theta$ vector, eight element rows the closest to the crack tip were selected with number 1 denoting the first element row, 2 the second element row and

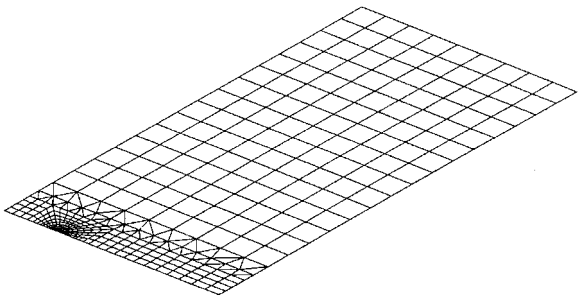

Fig. 3. Shell element model for the $G$ profile calculations by the presented method.

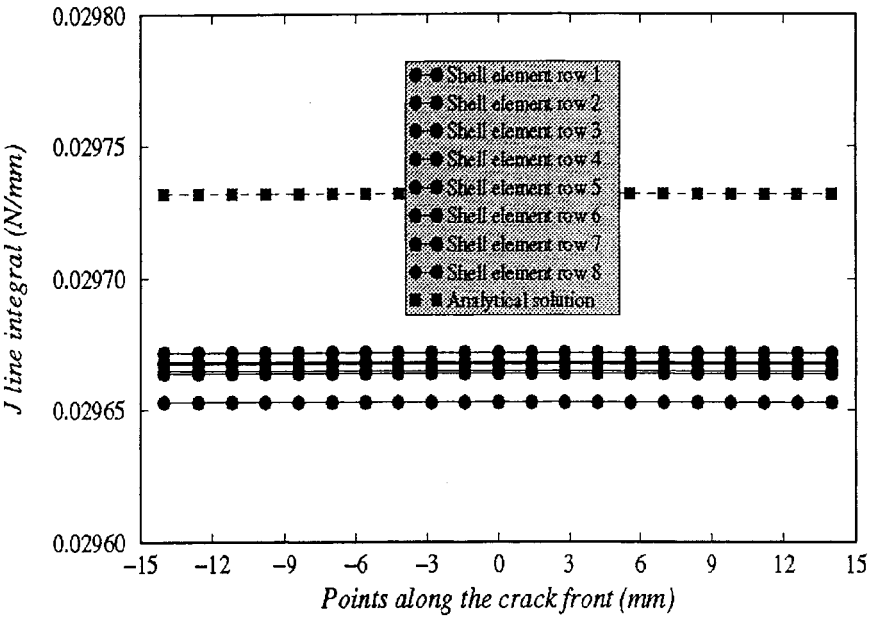


Fig. 4. *J*-integral profile (N/mm) by Eq. (16) along the crack front (mm) for the plate subjected to a pure membrane tension.

so on. Computed $G$ profiles along the crack front from Eq. (16) are summarized in Fig. 4. It is shown that the $G$ parameter is effectively constant in the plate's thickness direction. Furthermore, the obtained values are in very good agreement with the analytical solution and the $G$ profile is highly independent of the mapping vectors, with a relative undulation of less than 0.1 percent between the 1st and 8th element rows.

### 4.2. Elastic through-wall flawed plate subjected to bending moment

Fig. 5 shows the same plate problem as considered obviously. But the loading is due to a pure bending moment, $M_{\text{elastic}}$, uniformly applied at ends in such a manner that the maximal compressive stress, $-\sigma_{\max}$, on the top surface and the maximal tension stress, $\sigma_{\max}$, on the bottom surface of the plate reach 10 MPa. The bending moment itself is therefore:

$$M_{\text{elastic}} = \frac{We^2\sigma_{\max}}{3} = 1.829 \times 10^5 \text{ N} \times \text{mm}.$$

For the purpose of comparison, the classic node-by-node VCE method is applied to a 3D brick element model. Fig. 6 depicts the finite element mesh, which is built with 3720 eight-noded brick elements and 4347 nodal points. This 3D brick element model is composed of eight equal-thickness layers, having the same mesh density in the $x$–$y$ plane for each one as that used in the shell model (Fig. 3).

Computed $G$ profiles along the crack front from Eq. (16) are summarized in Fig. 7 for the eight element rows closest to the crack tip. Again, it is shown that, in elasticity, the $G$ profile is highly stable with a relative numerical undulation less than 0.1 percent when different mapping vectors are used. Comparisons of results by the shell and 3D brick element models are also conducted in Table 1, in which only solutions by the 8th element row for the $\Theta$ vector are given. There is a significant shift in the

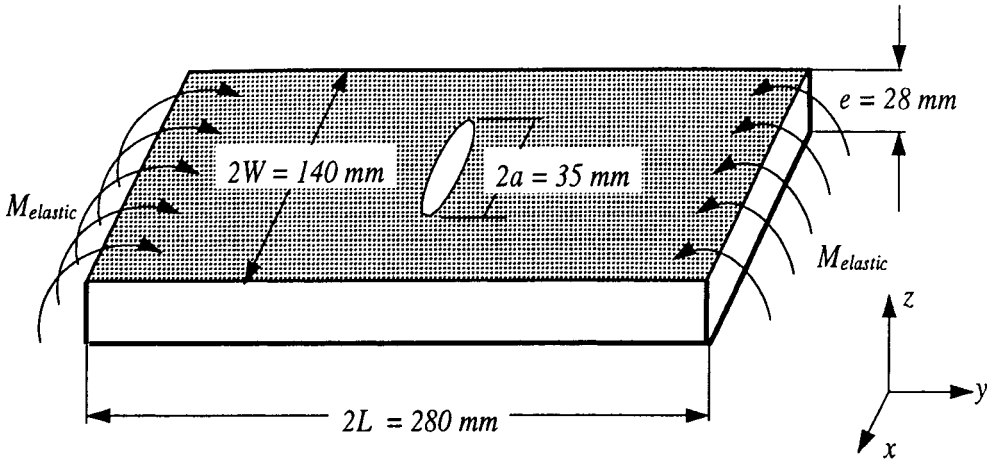


Fig. 5. Flawed plate subjected to a pure bending moment.

shell solution when compared to the 3D solution near the free edges. This is perhaps due to the plane stress type of behaviour near the free 3D surface, but plane strain type of behaviour near the core in thick plate/shell structures.

Negative values in Fig. 7 and in Table 1 indicate that under the pure bending moment, the superior half part of the crack (compressive side) is in shutting mode, only its inferior half part (tension side) is in opening mode. Normally, the method presented obviously cannot determine whether the crack is in shutting or in opening mode, since the strain energy density is always positive. In this illustrative example, negative signs were added afterwards. According to the results illustrated in Fig. 7 or in Table 1, it is concluded that the $J$-integral profile along the crack front in the thickness direction by the present method is very close to that by the 3D solid brick elements using the classic node-by-node VCE technique. Numerical scatter is less than 5 percent, except for those on the top and bottom surfaces, probably due to the boundary effect of the problem with the 3D brick elements. As an indication, we note that by the classic VCE method, the average value of the $J$-integral throughout the entire shell thickness equals $6.31 \times 10^{-3}$ N/mm, much less than the maximal value on the bottom surface of the

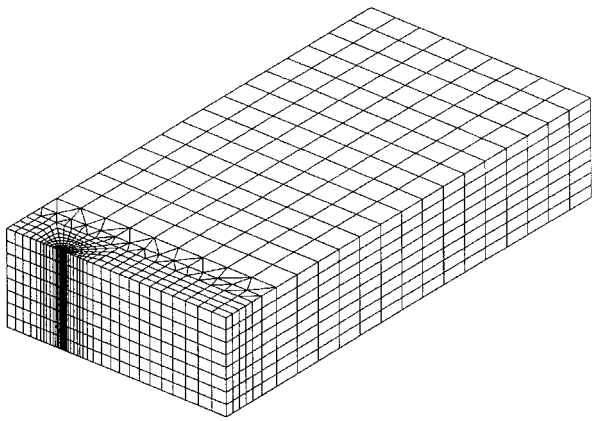

Fig. 6. 3D brick element model for the $G$ profile calculations by the classic node-by-node VCE method.

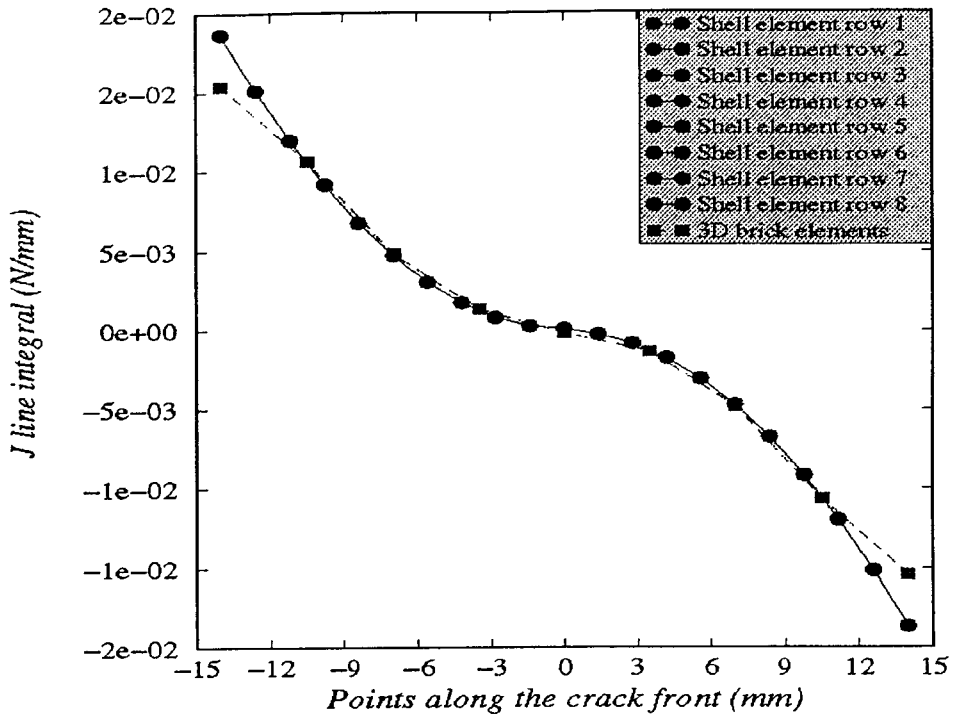


Fig. 7. *J*-integral profile (N/mm) by Eq. (16) along the crack front (mm) for the plate subjected to a pure bending moment.

plate ($1.875 \times 10^{-2}$ N/mm). This disagreement shows that an accurate evaluation of the *J*-integral at different levels on the crack front should be more desirable than a simple average evaluation, particularly in the cases where shell elements are subjected to a great deal of bending strain.

The calculations of the *J*-integral profile by the approximate formula (17) requires the selection of a shell element situated in crack's HRR-field controlled region, in which the multi-layer model will be established. Also, it requires the selection of a multi-layer number in such an element in order to determine the strain energy density evaluation over the whole transversal section. Taking a shell element situated in the first element row surrounding the crack tip, the *J*-integral on the bottom surface

Table 1
*J*-integral for some particular points on the crack front by Eq. (16)

| Coordinate *z* of points on the crack front | *J*-integral profile by shell elements | *J*-integral profile by 3D brick elements |
|---|---|---|
| −1.40000E+01 | 1.87482E−02 | 1.53954E−02 |
| −1.05000E+01 | 1.05813E−02 | 1.06228E−02 |
| −7.00000E+00 | 4.72733E−03 | 4.84312E−03 |
| −3.50000E+00 | 1.28931E−03 | 1.35377E−03 |
| 0. (middle plane) | 8.13548E−05 | 1.94906E−04 |
| 3.50000E+00 | −1.28932E−03 | −1.35377E−03 |
| 7.00000E+00 | −4.72735E−03 | 4.84312E−03 |
| 1.05000E+01 | −1.05813E−02 | 1.06228E−02 |
| 1.40000E+01 | −1.87482E−02 | −1.53954E−02 |

Table 2
*J*-integral (N/mm) on the bottom surface of the plate versus the number of multi-layers by Eq. (17)

| Number of multi-layers | *J*-integral on the bottom surface of the plate (N/mm) |
|---|---|
| 3 | 1.25577E−02 |
| 5 | 1.66950E−02 |
| 7 | 1.77801E−02 |
| 9 | 1.81939E−02 |
| 11 | 1.83920E−02 |
| 15 | 1.85681E−02 |
| 21 | 1.86630E−02 |
| 27 | 1.87005E−02 |
| 33 | 1.87190E−02 |
| 39 | 1.87295E−02 |
| 45 | 1.87360E−02 |
| 51 | 1.87403E−02 |
| 65 | 1.87461E−02 |

($z=-14$ mm) of the plate computed by a series of different multi-layer numbers are summarized in Table 2.

It is clearly seen that the *J*-integral profile or, more exactly, the area under the $w(z)$–$z$ curve composed of several piece-wise straight lines, becomes very independent of the multi-layer number when the latter is superior to 21. Nine multi-layers is somewhat the minimal number which leads to a scatter of about 3 percent when comparing its solution against the exact *J* value ($1.875 \times 10^{-2}$ N/mm) by Eq. (16).

Fig. 9 plots four *J*-integral solutions along the crack front which were obtained with a shell element

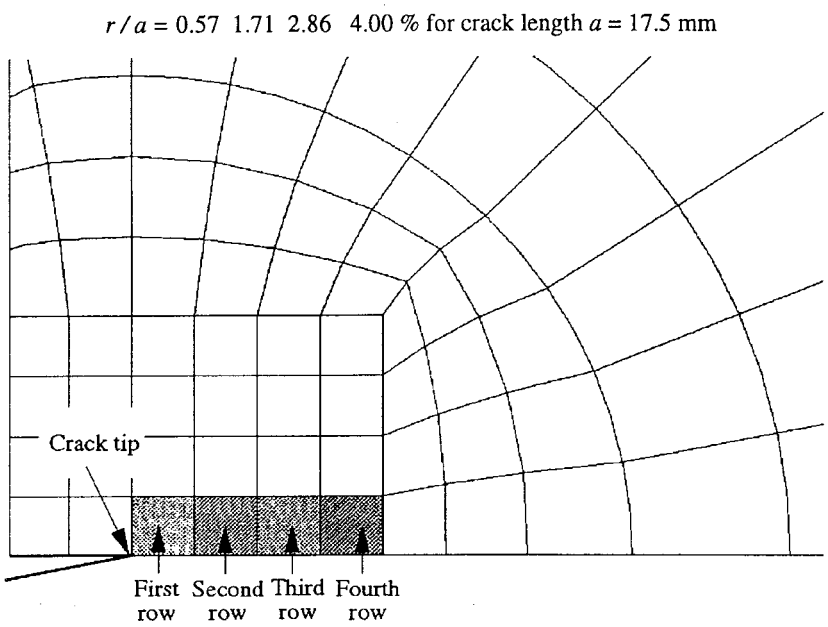


Fig. 8. Four different multi-layer-support elements in the HRR-field controlled region.

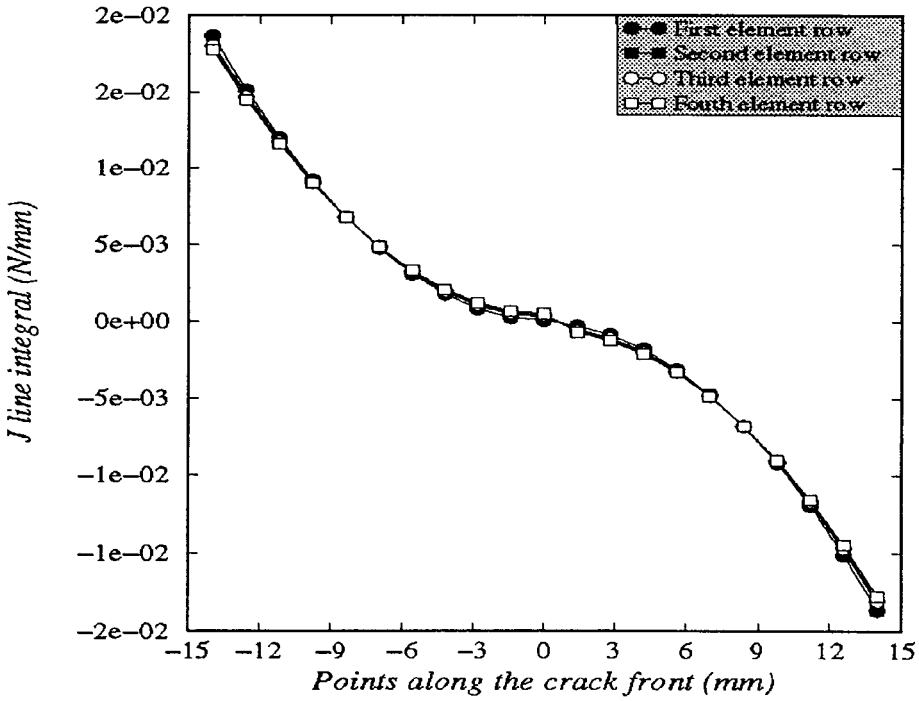


Fig. 9. *J*-integral profile by the four different multi-layer-support elements.

containing 21 multi-layers and located, respectively, in the first, second, third and fourth element row surrounding the crack tip as depicted in Fig. 8. The geometry center of these elements to the crack tip is:

$$\frac{r}{a} = 0.57\ 1.71\ 2.86 \sim 4.00\% \text{ for crack length } a = 17.5 \text{ mm}.$$

In addition, the values of the *J*-integral in Fig. 9 on the bottom surface ($z = -14$ mm) of the plate are also listed in Table 3. It follows that the element supporting the multi-layer model in the first, second and third element row leads to almost a same value for the *J*-integral with a numerical disagreement less than 3.5 percent. Clearly, in order to increase calculation accuracy it is preferable to define a multi-layer-support element which is, geometrically, neither too close to the crack tip nor too remote from it. In the first case, the strain and stress (hence the strain energy density) are in general computed with low calculation accuracy. In the second case, the HRR singular fields used as a base of the proportional

Table 3
*J*-integral (N/mm) on the bottom surface of the plate versus the distance of the multi-layer-support element to the crack tip $r/a$

| Distance of the multi-layer elements to the crack tip $r/a$ | *J*-integral on plate's bottom surface (N/mm) |
|---|---|
| 0.57% | 1.86630E−02 |
| 1.71% | 1.82012E−02 |
| 2.86% | 1.80121E−02 |
| 4.00% | 1.77682E−02 |

hypothesis risk losing their applicability because they were obtained from asymptotical solutions. This means that they are only available for points close enough to the crack tip. For the present problem, it seems that the most stable solution was due to the multi-layer-support element in the second row of shell elements.

### 4.3. Elastic–plastic through-wall flawed plate subjected to bending moment

In elastic–plasticity, the material behavior was modeled by the Ramberg–Osgood stress–strain representation of the following form:

$$\frac{\varepsilon}{\varepsilon_y} = \frac{\sigma}{\sigma_y} + \alpha\left(\frac{\sigma}{\sigma_y}\right)^n,$$

where $\sigma_y$ (400 Mpa) is a reference elastic stress, usually taken to be the yield stress, $\varepsilon_y$ ($2 \times 10^{-3}$) the corresponding yield strain. Respectively, $n$ (7.0) and $\alpha$ (1.0) are the material's work hardening exponent and yield offset.

The loading was always due to a pure bending moment, $M_{\text{appl}}$, increased monotonically so that the material's mechanical response followed the deformation theory of plasticity. Again, results obtained by the shell element model were compared against those by the 3D brick element model. At the end of the calculations, the applied moment reached 80 times the elastic bending moment, $M_{\text{elastic}}$ ($1.829 \times 10^5$ Nmm), considered in the preceding elastic calculations. At the final step, the plate was nearly fully plastified with an equivalent plastic strain at the crack tip region reaching 125 percent. Fig. 11 illustrates the evolution of the plastified region in the plate versus the applied moment.

To illustrate the independence of the $J$-integral profile with respect to the mapping vector $\Theta$, the computations by the shell element model were carried out using the same eight element rows the closest to the crack tip as in elastic case. However, for the 3D brick element model the $J$-integral profile along the crack front was derived using the 8th element row to support the vector $\Theta$ alone. Comparison of results by the two element models versus the applied bending moment is conducted in Fig. 12. It is seen that the $J$-integral profile is highly independent of the mapping vector $\Theta$, representing a numerical undulation less than 2 percent in the maximal loading case $M_{\text{appl}} = 80\ M_{\text{elastic}}$. As the plasticity increases, the $G$ profile from the shell model becomes nearly linear. This is due to the fact that when the plate is highly plastified, the stress varies almost linearly along the crack front with the given stress–strain relationship. The variation of both the strain energy density and, therefore, the $G$ profile are linear along this line.

The $J$-integral solutions on the bottom surface of the plate by the two finite element analysis are plotted in Fig. 10 against the applied bending moment. We note that the $J$-integral comes from the multi-layer shell element model is in very good agreement with the solutions of the 3D brick element analysis throughout the whole range of elastic–plastic deformation. Such a comparison provides an additional verification of the calculation method of the $J$-integral profile along the crack front using the multi-layer shell element developed in the present investigation.

## 5. Discussions and conclusions

A numerical approach is described in the present paper for calculating the energy release rate (or the $J$-integral) along any crack front in the thickness direction of shell elements. For this purpose, it is assumed that the energy release rate at any level in the crack front is linearly proportional to the strain energy density of points at the same level in the region where HRR singular fields are dominant. In

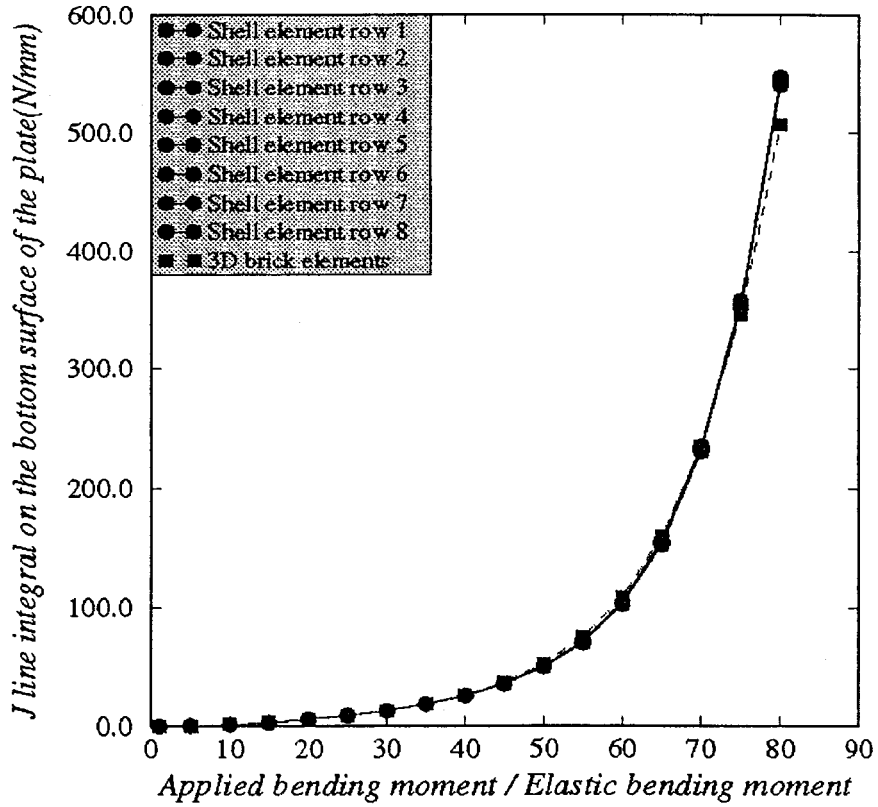


Fig. 10. Comparison of the $J$-integral on the bottom surface of the plate versus the bending moment.

elastic–plasticity, the method requires the selection of a single shell element being modeled in multi-layers to determine the strain energy density evolution throughout the whole transversal section. It is recommended to select a multi-layer-support element which is, geometrically, neither too close to the crack tip nor too remote from it and contains at least 21 equal-thickness slim layers for the purpose of calculation accuracy. Illustrative examples were made for a through-wall flawed plate problem. Computed $J$-integral results have been found to be highly independent of integration paths and have been compared against those by a 3D brick element model using the classic node-by-node VCE method. It was observed that the $J$-integral profile by the present method is in good agreement with that by the 3D brick finite element analysis throughout the entire range of elastic–plastic deformation.

The principle of the method may easily be extended for calculating other fracture characteristic integrals like the $C*$ or $C(t)$ integrals used in creep fracture problems (Landes and Begley, 1976; Riedel, 1981). In such a case, it suffices to replace the strain energy density variation by the strain energy rate density variation over the shell's thickness. Note that no particular assumptions have been made about the crack's fracture mode. The method is hence suitable for cracks in pure I, II and III opening mode, or in their mixed fracture mode. The use of the numerical process is, however, limited by the applicability of the HRR singular fields (Hutchinson, 1968; Rice and Rosengren, 1968) with some theoretical difficulties, as is well known in plane strain/stress problems. For computation accuracy, it is recommended to model crack's singular region with fine and regular high order elements.

The multi-layer shell element model developed in this investigation can also conveniently be used for

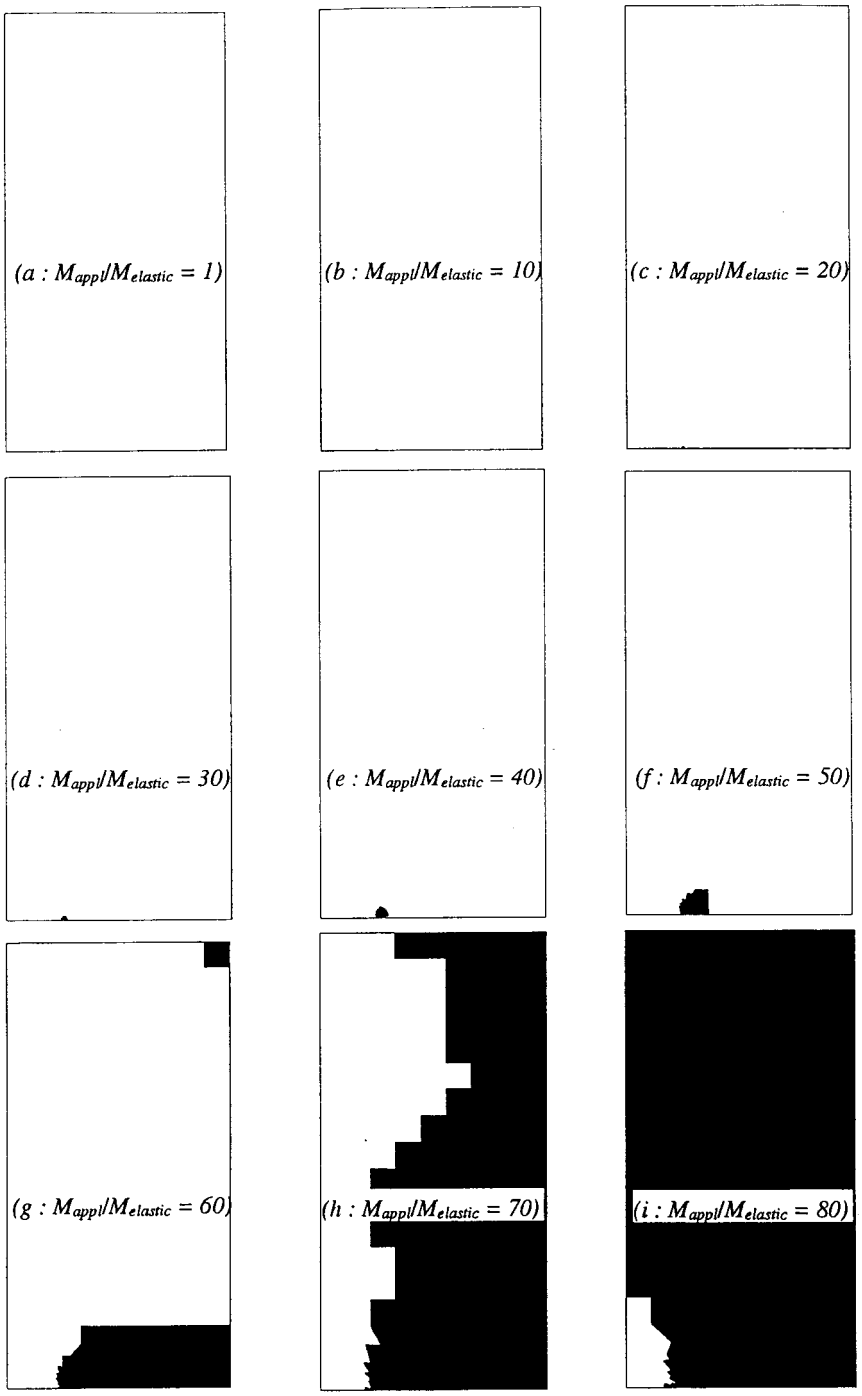


Fig. 11. Evolution of the plastified region versus the applied bending moment.

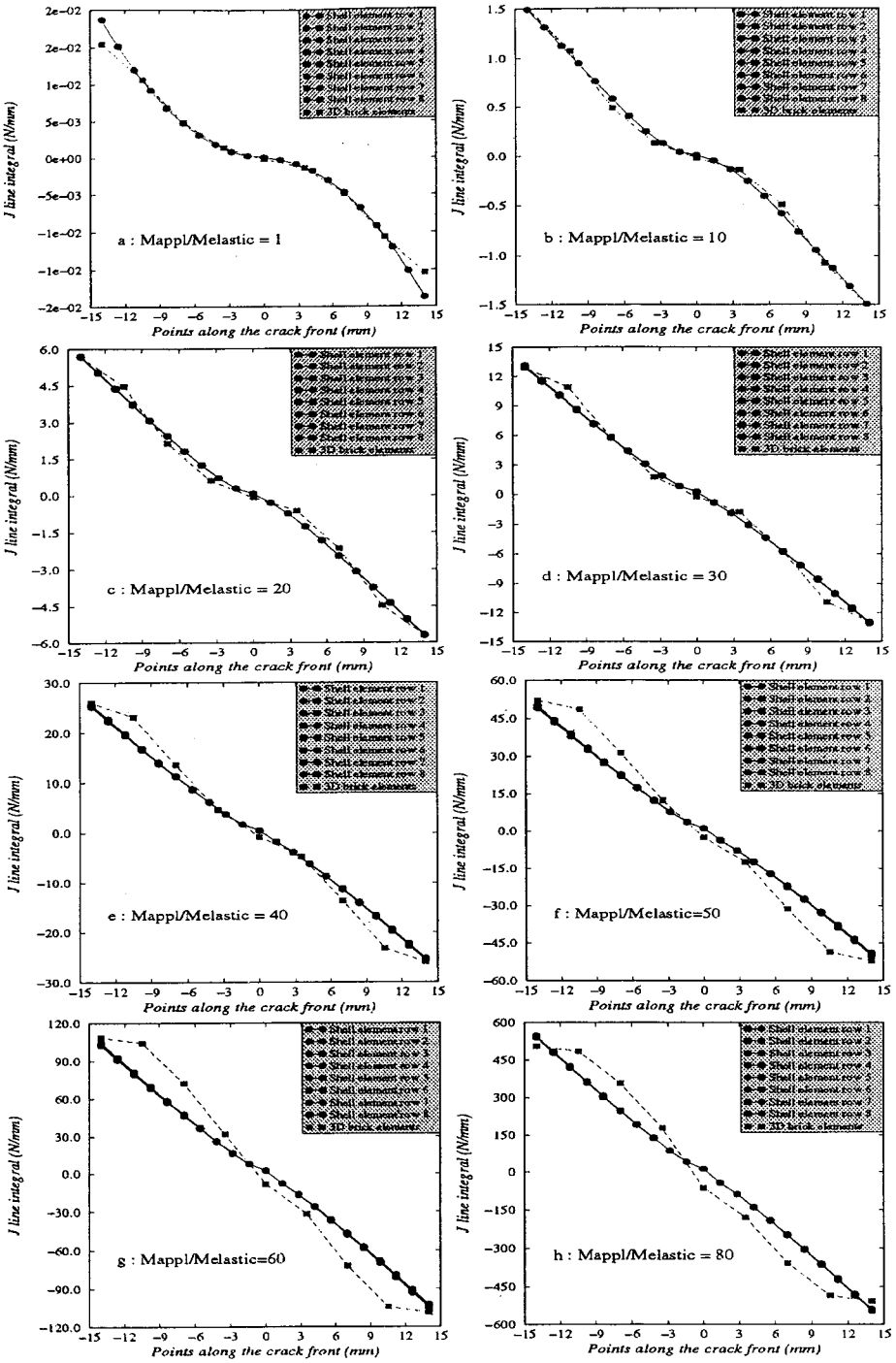


Fig. 12. *J*-integral profile along the crack front versus the bending moment.

the response of thin walled structures of composite materials without relative movement between different layers. In such a case, the master stiffness matrix should be obtained by assembling that one of all elements at each individual level since material's characteristics are distinct at different levels. When using this element model for crack problems, attention should be paid to cracks in closure mode because of the inconsistency between Kirchhoff's hypothesis about the straight transverse line and the real deformation. For instance, in the case of the plate under pure bending moment shown in our examples, the inferior half part of the crack (tension side) is in opening mode, but its superior half part (compressive side) is in shutting mode. Normally, unilateral contact conditions in the direction of middle surface are necessary along the crack's compressive side for an accurate stress/strain analysis, so that lines in the contact region cannot remain rigorously straight after the plate's deformation, as expected in Kirchhoff's shell theory. However, it seems that the ignorance of these conditions has no significant effect on the stress/strain far from the crack-tip since the displacement in the plane of the elements due to the crack closure is much less than the plate's transversal displacement. This is particularly true when very thin plate is calculated. Such an ignorance was also justified by a comparative calculation performed for the 3D brick element model where very close results have been derived between the analyses with and without the unilateral contact conditions.

When using multi-layer shell elements, the thickness of the structure is, in general, considerably less than the structure's characteristic dimensions and a single nodal point suffices to model the crack front. For this reason, the latter has been reasonably assumed in our investigations to be a straight line and normal to the middle surface. It has also been assumed to penetrate throughout the entire transversal section. Otherwise, the proposed method will not be applicable any further and, in this case, we have to use a 3D brick element model for calculating the $J$-integral profile along the crack front.

## Acknowledgements

The financial support shared among Commisariat de l'Energie Atomique (CEA), Electricit de France (EDF) and NOVATOME–FRAMATOME to the present research work is gratefully acknowledged.

## References

Batoz, J.L., Dhatt, G., 1990. Modélisation Des structures par Eléments Finis. Hermés, Paris.

De Lorenzi, H.G., 1982. On the energy release rate and the $J$-integral in 3-D crack configurations. Int. J. of Fracture 19, 183–193.

Destuynder, Ph., Djaoua, M., 1981. Sur une interprétation mathématique de l'intégrale de Rice en théorie de la rupture fragile. Math. Meth. in the Appl. Science 3, 70–87.

Haber, R.B., Koh, H.M., 1985. Explicit expressions for energy release rate using virtual crack extensions. Int. J. for Num. Methods in Engineering 21, 301–315.

Hellen, T.K., 1975. On the method of virtual crack extension. Int. J. for Num. Methods in Engineering 9, 187–207.

Hellen, T.K., 1989. Virtual crack extension methods for non-linear materials. Int. J. for Num. Methods in Engineering 28, 929–942.

Hutchinson, J.W., 1968. Singular behavior at end of tensile crack in hardening material. Mech. Phys. Solids 16, 1–12.

Ishikawa, H., 1980. A finite element analysis of stress intensity factors for combined tensile and shear loading by only a virtual crack extension. Int. J. of Fracture 16, R243–R246.

Isida, M., 1955. On the Tension of a strip with a central elliptical hole. Tran. Jap. Soc. Mech. Engineering 21, 37–49.

Landes, J.D., Begley, J.A., 1976. Crack tip fields under non-steady creep crack growth mechanics of crack growth. ASTM STP 590, 128–148.

Nikishkov, G.P., Atluri, S.N., 1987. Calculation of fracture mechanics parameters for an arbitrary three-dimensional crack by the 'equivalent domain integral' method. Int. J. for Num. Methods in Engineering 24, 1801–1821.

Pryor, C.W., Barker Jr., R.M., Frederick, D., 1970. Finite element bending analysis of Reissner plates. J. Eng. Mech. Div., ASCE, 967–983.

Parks, D.M., 1974. A stiffness derivative finite element technique for determination of crack tip stress intensity factors. Int. J. of Fracture 10 (4), 487–502.

Parks, D.M., 1977. The virtual crack extension method for nonlinear material behavior. Computer Methods Appl. Mech. Engineering 12, 353–364.

Rice, J.R., Rosengren, G.F., 1968. Plane strain deformation near crack tip in power-law hardening material. J. Mech. Phys. Solids 16, 13–31.

Riedel, H., 1981. Creep deformation at crack tips in elasto–viscoplastic solids. J. Mech. Phys. Solids 29, 35–49.

Sha, G.T., Yang, C.T., 1985. Weight function calculations for mixed-node fracture problems with the virtual crack extension technique. Eng. Fracture Mechanics 21, 1119–1150.

Suo, X.Z., Combescure, A., 1992a. Double virtual crack extension method for crack growth stability assessment. Int. J. of Fracture 57 (2), 127–150.

Suo, X.Z., Combescure, A., 1992b. On the application of $G(\Theta)$ method and its comparison with De Lorenzi's approach. Nuc. Engg. and Design 135, 207–224.